Published in final edited form as:
Neuroscience. 2007 February 9; 144(3): 1094–1108.

Calcium permeable AMPA receptors and autoreceptors in external tufted cells of rat olfactory bulb

Jie Ma and **Graeme Lowe**
Monell Chemical Senses Center, Philadelphia, PA

Abstract

Glomeruli are functional units of the olfactory bulb responsible for early processing of odor information encoded by single olfactory receptor genes. Glomerular neural circuitry includes numerous external tufted (ET) cells whose rhythmic burst firing may mediate synchronization of bulbar activity with the inhalation cycle. Bursting is entrained by glutamatergic input from olfactory nerve terminals, so specific properties of ionotropic glutamate receptors on ET cells are likely to be important determinants of olfactory processing. Particularly intriguing is recent evidence that α-amino-3-hydroxy-5-methylisoxazole-4-propionic acid (AMPA) receptors of juxta-glomerular neurons may permeate calcium. This could provide a novel pathway for regulating ET cell signaling. We tested the hypothesis that ET cells express functional calcium-permeable AMPA receptors. In rat olfactory bulb slices, excitatory postsynaptic currents (EPSCs) in ET cells were evoked by olfactory nerve shock, and by uncaging glutamate. We found attenuation of AMPA/kainate EPSCs by 1-naphthyl acetyl-spermine (NAS), an open-channel blocker specific for calcium permeable AMPA receptors. Cyclothiazide strongly potentiated EPSCs, indicating a major contribution from AMPA receptors. The current-voltage (I-V) relation of uncaging EPSCs showed weak inward rectification which was lost after > ~ 10 min of whole-cell dialysis, and was absent in NAS. In kainate-stimulated slices, Co^{2+} ions permeated cells of the glomerular layer. Large AMPA EPSCs were accompanied by fluorescence signals in fluo-4 loaded cells, suggesting calcium permeation. Depolarizing pulses evoked slow tail currents with pharmacology consistent with involvement of calcium permeable AMPA autoreceptors. Tail currents were abolished by Cd^{2+} and NBQX, and were sensitive to NAS block. Glutamate autoreceptors were confirmed by uncaging intracellular calcium to evoke a large inward current. Our results provide evidence that calcium permeable AMPA receptors reside on ET cells, and are divided into at least two functionally distinct pools – postsynaptic receptors at olfactory nerve synaptic terminals, and autoreceptors sensitive to glutamate released from dendrodendritic synapses.

Keywords

glutamate; glomerulus; dendrite; uncaging; fluorescence; rectification

Olfaction begins with the binding of odorants to olfactory receptors which transduce sensory input into action potentials in axons of the olfactory nerve. Axons of cells expressing the same receptor gene converge to stereotypic glomeruli in the superficial layer of the olfactory bulb, forming a topographic neural map of receptor activation (Mombaerts et al., 1996). The olfactory nerve terminals make direct excitatory synapses on dendrites of bulb output neurons,

Address correspondence to: Dr. Graeme Lowe, Monell Chemical Senses Center, 3500 Market St, Philadelphia, PA 19104-3308, phone: 215-573-5110, fax: 215-898-2084, email: loweg@monell.org.

mitral and tufted cells. The glomeruli, however, are more than simple relays for an unprocessed sensory map. They encapsulate a dense tangle of dendrodendritic microcircuitry originating from a surrounding shell of diverse inhibitory interneurons, including several types of periglomerular cells and short axon cells. During odor information processing, these interneurons can mediate both recurrent inhibition in the same glomerulus (Murphy et al., 2005), and lateral inhibition between different glomeruli (Aungst et al., 2003).

Another major element of the glomerular circuitry is a specialized class of principal neurons, the external tufted (ET) cells. Dendritic tufts of ET cells arborize extensively inside glomeruli, where they receive monosynaptic glutamatergic input from olfactory nerve terminals (Hayar et al., 2004a). In slices, ET cells exhibit spontaneous burst firing driven by a persistent sodium current. Paired recordings show that multiple ET cells projecting to the same glomerulus have their bursts synchronized, and that this synchrony likely depends on correlated synaptic inputs as well as gap junction couplings (Hayar et al., 2005). The bursting can be entrained by theta-frequency (5 – 10 Hz) activation of olfactory inputs, as would occur during repetitive sampling of odorants by sniffing (Hayar et al., 2004b). Therefore, a primary function of ET cells may be to coordinate and maintain the temporal coherence of glomerular network dynamics during odor processing at the sniff frequency. This coordination would hinge on the potent excitatory drive that individual ET cells exert on periglomerular cells through dendrodendritic synapses. Glutamate released from the dendrite of one ET cell can depolarize many periglomerular cells, triggering reciprocal GABA release in an oscillatory negative feedback loop (Murphy et al., 2005). Thus, fast glutamatergic neurotransmission is critical for ET cell circuit operations in both presynaptic and postsynaptic contexts. Determining the specific physiological properties of glutamate receptors expressed by ET cells is an important step towards a better understanding of their function.

Ionotropic glutamate receptors are expressed in a diversity of forms (Dingledine et al., 1999), and recent studies have indicated localization of different subtypes in distinct compartments of olfactory bulb neurons (Trombley and Shepherd, 1993; Montague and Greer, 1999; Blakemore and Trombley, 2003; Lowe, 2003; Horning et al., 2004). In the glomerular layer of the bulb, both NMDA and AMPA/kainate receptors have been characterized by immunolabeling (Giustetto et al., 1997; Montague and Greer, 1999; Sassoe-Pognetto et al., 2003) and physiological studies (Ennis et al., 1996; Aroniadou-Anderjaska et al., 1997; Keller et al., 1998; Edwards and Michel, 2003; Murphy et al., 2004). Of particular interest are AMPA receptors that either lack the GluR2 subunit, or assemble with an unedited version of that subunit (Ozawa et al., 1998). These receptors have a high calcium permeability because the GluR2 subunit normally blocks Ca^{2+} entry when its primary transcript has been edited (Hume et al., 1991; Egebjerg and Heinemann, 1993). Calcium permeation offers an additional signal transduction pathway, in parallel with membrane depolarization, through which AMPA receptors can influence or control neuronal functions. A recent study using cultured cells and slices reported direct evidence for the expression of calcium permeable AMPA receptors in olfactory bulb neurons. In the glomerular layer of slices, unidentified neurons (collectively termed juxtaglomerular cells) were found to take up Co^{2+} ions (which selectively permeate calcium permeable AMPA receptors) and their postsynaptic responses to olfactory nerve shock were blocked by 1-naphthyl acetyl-spermine (NAS), a selective antagonist of calcium permeable AMPA receptors (Blakemore et al., 2006).

In our study, we specifically targeted ET cells in slices for electrophysiological and optical recording to determine if they expressed calcium permeable AMPA receptors. We examined the pharmacology and voltage dependence of excitatory postsynaptic currents (EPSCs) activated either by glutamate released from olfactory nerve terminals, or by exogenously applied glutamate. Intracellular Ca^{2+} transients associated with these EPSCs were detected by fluorometry. Our results indicate the presence of calcium permeable AMPA receptors at both

conventional olfactory nerve-ET cell axodendritic synapses, and at dendrodendritic synapses. In the latter case, glutamate liberated from ET cell dendrites activated AMPA autoreceptors on the same cell, and these receptors may be of the Ca^{2+} permeable type. All experimental procedures complied with U.S. Public Health Service guidelines for the humane use and care of laboratory animals. The number of animals used was minimized and pain was alleviated with anesthetics.

EXPERIMENTAL PROCEDURES

Slice preparation

Olfactory bulb slices were prepared and visually identified cells recorded with techniques similar to those previously described (Lowe, 2002; Ma and Lowe, 2004). Briefly, male rats (P21-42, CD, Charles River Laboratories, Wilmington, MA) were sacrificed by decapitation while anaesthetized either by halothane inhalation, or by sodium pentobarbital (50–65 mg/kg, i.p.) followed by transcardial perfusion of ice-cold, oxygenated sucrose slicing solution (mM): 240 sucrose, 2.5 KCl, 10 Na-HEPES, 10 glucose, 1 $CaCl_2$, 4 $MgCl_2$, 0.2 ascorbic acid, pH 7.2. (3 min). Horizontal bulb slices (200 – 300 μm) were cut in the same sucrose solution and slices were incubated for 1–3 h (32°C–23°C) in an interface chamber with high Mg^{2+} artificial cerebrospinal fluid (ACSF) (mM): 124 NaCl, 2.5 KCl, 26 $NaHCO_3$, 1.25 NaH_2PO_4, 10 glucose, 1 $CaCl_2$, 3 $MgCl_2$ (95% O_2, 5% CO_2). For recording, slices were submerged in an open chamber, immobilized with a platinum harp and perfused (2 ml/min) with standard artificial cerebrospinal fluid (mM): 124 NaCl, 2.5 KCl, 26 $NaHCO_3$, 1.25 NaH_2PO_4, 25 glucose, 2 $CaCl_2$, 1.3 $MgCl_2$ (95% O_2, 5% CO_2, 23°C). In some experiments requiring bath Cd2+, $NaHCO_3$ was replaced with equimolar sodium HEPES buffer. Extracellularly applied drugs were delivered by switching the perfusion source in open flow perfusion, or by injection into the chamber in recycled flow perfusion (concentration in bulk solution stabilized after 5 min). Drugs used included: R-2-amino-5-phosphonopentanoate (APV), tetrodotoxin (TTX), tetraethylammonium chloride (TEA), 4-aminopyridine, bicuculline methiodide (BMI), 5,7-dichlorokynurenic acid (dCK), (±)-4-(4-aminophenyl)- 2,3-dioxo-6-nitro-1,2,3,4-tetrahydrobenzo[f]quinoxaline-7-sulfonamide (NBQX) disodium, 6-chloro-3,4-dihydro-3-(2-norboren-5-yl)-2H-1,2,4-benzothiazidiazine-7-sulfonamide-1,1-dioxide (cyclothiazide, CTZ), 1-naphthyl acetyl-spermine (NAS), (+)-α-methyl-4-carboxyphenylglycine (MCPG), kainic acid (Sigma-Aldrich, St Louis, Missouri), and 1,2-dihydro-1-methyl-2-propylcarbamoyl-6,7-methylenedioxyphthalazine (SYM2206) (Tocris Bioscience, Ellisville, Missouri).

Electrophysiology

Whole-cell recording pipettes (4–8 MΩ) were filled either with a potassium methylsulfate internal solution (mM): 122 K-CH_3SO_4, 5 KCl, 26 K-HEPES, 2 Mg-ATP, 0.3 Na-GTP, 1 $MgCl_2$, 4 Na_2-phosphocreatine, 6.5 biocytin HCl (pH 7.2); or a Cs-methanesulfonate based solution (mM): 130 $CsMeSO_3$, 5 NaCl, 24 Na-HEPES, 0.2 K-EGTA, 2 Mg-ATP, 0.3 Na-GTP, 1 $MgCl_2$, 4 Na_2-phosphocreatine, 6.5 biocytin (pH 7.2). In studies of the autoreceptor current, 30 mM of the methanesulfonate anion was replaced by glutamate, which stabilized the current against transmitter depletion. Holding potentials in voltage clamp were corrected for liquid junction potentials using JPCalc software (Barry, 1994). In some cells, 10 mM N-(2,6-dimethylphenylcarbamoylmethyl) triethylammonium bromide (QX314) (Sigma) was added to the internal solution to block Na^+ currents. A few cells were also recorded by the perforated-patch method (pipettes included 0.2 mg/ml gramicidin). Somata of ET cells were visualized with differential interference contrast (DIC) optics using either an Olympus BX50-WI microscope with a 60× NA 0.90 water immersion objective, or Nikon E600 FN microscope with a Leica 63X/NA 0.90 water immersion objective. Voltage-clamp currents were recorded with an Axopatch-1D amplifier (Axon Instruments, Union City, California) controlled by Pulse

8.5 software (HEKA Electronik, Lambrecht, Germany), or an EPC-8 patch-clamp amplifier (HEKA Electronik) controlled by custom software written in LabVIEW (National Instruments, Austin, Texas). Our standard protocol following patch rupture was to wait 5 min to stabilize series resistance, allowing time for fluorescent dye to load into the dendrite to verify the ET cell morphology. Initial control responses were recorded immediately before introducing drugs into the perfusion system. Whenever EPSC amplitudes and whole-cell input resistance both declined sharply during a recording session, or if series resistance was too unstable, data from the cell were rejected. At various times during extended recording sessions (≥ 15 min), series resistance was measured by applying − 30 mV voltage test pulses, and minor corrections to the AMPA receptor current were calculated off-line by assuming an approximately linear I-V relation for inward currents and a standard reversal potential of + 10 mV (Fig. 3A). After each experiment, if recorded cells were intact the slices were fixed overnight (4°C) in phosphate-buffered saline with 2% glutaraldehyde. Dendritic arbors were stained by treatment with Vectastain Elite ABC kit, and VIP peroxidase substrate kit (Vector Laboratories, Burlingame, California), slices cleared as whole mounts in 80% glycerol, and cells examined under a Nikon Microphot microscope with digital camera. Dendrites of putative ET cells were also visualized during recording by intracellular loading of fluorescent dyes (Calcium Orange, Alexa Fluor 594 or 647) (Molecular Probes, Eugene, Oregon) from the whole-cell pipette.

Stimulation

For stimulation of ET cells by olfactory nerve shock, a concentric bipolar platinum/iridium electrode (125 μm outer pole, 25 μm inner pole) (Frederick Haer & Co, Bowdoinham, Maine) was positioned in the overlying olfactory nerve layer and 100 – 200 μs, 0.2 – 0.4 mA pulses applied by a constant current generator (A320, World Precision Instruments, Sarasota, Florida). For glutamate uncaging, 500 μM – 1 mM 4-methoxy-7-nitroindolinyl (MNI-) glutamate (Tocris) was added to the bath, and uncaged by one of three light sources: a xenon flash lamp (Cairn Research Ltd, Faversham, UK), an Innova 90C argon ion laser (Coherent Inc, Santa Clara, California) or a pulsed nitrogen laser (VSL-337ND-S, Laser Science Inc, Cambridge, Massachusetts). Uncaging light was steered through the water immersion objective by a dichroic mirror (505DRLPXR, Omega Optical, Brattleboro, Vermont). Broad spectrum emission from the flash lamp (0.5 ms half duration pulses) was relayed by a 3 mm diameter liquid light guide, while the laser beams were propagated in free space. Laser uncaging was confined to a focal area near the soma or dendrite, whereas the flash lamp uncaged over a larger area. In the case of focal uncaging, lateral diffusion of glutamate released after a laser flash was expected to activate receptors outside the focal spot.

A rough estimate of the concentration of glutamate released by flash lamp uncaging was obtained by comparing AMPA receptor currents (at − 60 mV) evoked by uncaging to those evoked by pressure ejection of known concentrations of L-glutamate (5, 10, 15, 20 μM) from a micropipette (8 MΩ). For these calibrations, we used the somata of CA1 pyramidal neurons in coronal hippocampal slices as a convenient source of AMPA receptors. The bath included 100 μM CTZ to block receptor desensitization, and 15 μM dCK to eliminate the NMDA receptor component of the current. Glutamate puffer solutions were made up in ACSF with $NaHCO_3$ buffer replaced by Na-HEPES, and 150 μM Alexa Fluor 594 to verify that the ejected bolus enveloped the soma (~ 3 – 4 somatic diameters). The AMPA receptor currents were extracted by subtracting the residual responses remaining after application of an AMPA receptor-specific inhibitor (100 μM SYM2206). The AMPA receptor current evoked by uncaging 500 μM MNI-caged glutamate was found to be bracketed by currents evoked by 5 μM and 10 μM glutamate (n = 4). We concluded that the flash lamp uncaging efficiency was about 1 – 2%.

Pressure ejection was not used to calibrate glutamate released by the nitrogen laser, as the diameter of the laser spot in the focal plane (~ 15 μm) was smaller than the diameter of a glutamate puff. Instead, we directly compared flash lamp and laser evoked currents in the same outside-out patches pulled from the somata of CA1 neurons and concluded that the N_2 laser uncaged approximately 30% of the glutamate released by the flash lamp (0.3% – 0.6%; 1.5 – 3 μM released glutamate; 300 μJ, 4 ns laser pulse). To estimate the glutamate uncaged by the argon laser, we calculated photolysis of MNI-caged glutamate by a Gaussian beam model developed previously (Lowe, 2003). In a region around the cell, ±10 μm above and below the focal plane, at incident power of 0.25 – 0.5 mW (5 ms flash), the uncaging was > 97% within the $1/e^2$ beam radius (< 2 μm), so initial uncaged glutamate was ~ 1 mM. After a delay of ΔT ~ 35 ms (mean rise time of uncaging EPSCs in CTZ), this column of glutamate expands by diffusion to a radius of ~ 2 μm + $\sqrt{(4D\Delta T)}$ ~ 12 μm, a 6-fold expansion ($D = 7.6 \times 10^{-5}$ cm^2s^{-1}), which dilutes the concentration of glutamate from 1 mM to 1/36 mM ~ 30 μM at the peak of the EPSC.

Cobalt labeling

For cobalt uptake and visualization, slices were: (i) perfused for 20 min (at 23°C) in artificial cerebrospinal fluid containing: 0.5 μM TTX, 100 μM dCK, 100 μM APV, 250 μM kainate, 5 mM $CoCl_2$; (ii) perfused for 10 min in divalent free artificial cerebrospinal fluid with 5 mM EDTA; (iii) rinsed and incubated for 5 to 6 min in 0.12% $(NH_4)_2S$ in artificial cerebrospinal fluid; and (iv) rinsed in artificial cerebrospinal fluid and fixed overnight in 4% paraformaldehyde, 0.1 M phosphate buffered saline at 4°C.

Fluorometry

For fluorometric measurement of Ca^{2+} transients, pipette solutions included 150 μM fluo-4 (K_5 salt; Molecular Probes, Oregon) and 100 μM Alexa Fluor 647. The long wavelength fluorescent dye was included to assist visualization of cell morphology with the aid of a low-light CCD video camera (V-1070, Marshall Electronics, El Segundo, California). Fluorescence was excited by a Nikon HB-10104AF 100 W Hg arc lamp. Filters used for fluo-4 were: excitation 470AF50 (XF1087), dichroic 500DRLP (XF2077), emission 545AF75 (XF3105); for Alexa Fluor 647: excitation 630AF50 (XF1069), dichroic 650DRLP (XF2035), emission 695AF55 (XF3076) (Omega Optical, Brattleboro, VT). Illumination at the cell was attenuated by neutral density filters and gated by a Uniblitz electronic shutter (Vincent Associates, Rochester, New York). To record Ca^{2+} signals, fluo-4 fluorescence from the cell (soma + proximal dendrite) was collimated and focused onto an avalanche photodiode detector (Photomax 200, Dagan Corporation, Minneapolis, Minnesota), with bias voltage 175 V, run in non-integrating mode. Detector readout was digitized by custom LabVIEW software. To stimulate cells, glutamate was uncaged with the argon laser with intensity attenuated to avoid generating a flash artifact in the photodiode (Fig. 4A).

Data analysis

Data were analyzed using Pulse 8.5 (HEKA Elektronik) and Origin 7.0 software (OriginLab, Northampton, Massachusetts). Summary results are expressed as mean ± S.E.M. unless otherwise stated. Rectification in current-voltage (I-V) relations was quantified by calculating a rectification index (RI), defined here as the ratio: RI = slope of I-V curve for V > 0/slope of I-V curve for V < 0 (slopes obtained by linear regression in each region). The definition is similar to that used by other authors, who compared chord slopes for inward and outward currents at −60 mV and +40 mV (Koike et al., 1997). Amplitudes of fluo-4 fluorescence transients were obtained after subtracting a bleaching curve estimated by linear fit of the prestimulus baseline photodiode output, or of control traces acquired without uncaging stimulation.

RESULTS

Olfactory nerve stimulation activates a polyamine-sensitive EPSC in ET cells

Identification of ET cells was based on a combination of morphological and physiological criteria established in previous studies (Pinching and Powell, 1971; Aungst et al., 2003; Hayar et al., 2004a). The ET cells tend to be distributed along the lower half of the glomeruli and their somata have larger diameters than periglomerular cells. They elaborate extensively branched dendritic tufts occupying much of the volume of a glomerulus, and cell-attached patch recordings of spontaneous activity often reveal a rhythmic bursting discharge pattern (Fig. 1A). Although experimental conditions (use of TTX to block Na^+ channels) did not allow us to observe bursting in all recorded cells, we selected for analysis cells which lacked secondary dendritic projections, that a recent study found was correlated with the burst firing property (Antal et al., 2006). Most ET cells had input resistances < 500 MΩ, lower than other classes of juxta-glomerular neurons.

Postsynaptic currents in ET cells were studied by obtaining whole-cell voltage-clamp recordings from the soma, held at − 60 mV. Cells were dialyzed with 10 mM QX314 from the pipette, to prevent activation of Na^+ channels by large depolarizing currents in fine dendrites (Isaac and Wheal, 1993). Under these conditions, the mean input resistance was 185 ± 23 MΩ (n = 10). In many cells, we observed spontaneous synaptic currents (Fig. 1A). For controlled activation of synaptic inputs we placed a bipolar stimulus electrode on the olfactory nerve layer superficial to the glomeruli near the recorded cell and delivered single extracellular current pulses. To isolate the current produced by AMPA/kainate receptors, NMDA receptors were blocked by bath application of either 100 μM APV or 15 μM dCK, and bicuculline was also included to block $GABA_A$ receptors. Under these conditions, olfactory nerve stimulation evoked large, short latency monophasic EPSCs in all cells morphologically classified as ET cells (peak amplitude 1232 ± 262 pA, latency 2.32 ± 0.09 ms, n = 29 cells). The short, invariant latency is consistent with the recruitment of monosynaptic inputs, so we interpreted the EPSCs as responses to neurotransmitter released directly from olfactory nerve terminals. The EPSCs had times to peak of 1.16 – 6.59 ms (3.05 ± 0.30 ms) and 50% decay times of 5.8 – 178 ms (37.63 ± 7.21 ms) (n = 29). The olfactory nerve-shock response was abolished by addition of 1 μM NBQX (n = 2), an antagonist of AMPA/kainate receptors. This is consistent with previous studies that have identified glutamate as the neurotransmitter and AMPA/kainate as postsynaptic receptors at olfactory nerve sensory terminals on mitral cells (Berkowicz et al., 1994; Ennis et al., 1996; Aroniadou-Anderjaska et al., 1997) and on ET cells (Murphy et al., 2004).

To test for the involvement of calcium permeable- (CP-) AMPA receptors, we used a synthetic Joro spider toxin analog, 1-naphthyl acetyl-spermine (NAS). This polyamine toxin acts as an open channel blocker that selectively antagonizes calcium permeable AMPA/kainate receptors (Asami et al., 1989; Ajima et al., 1991). After recording stable control responses, the perfusion solution was switched to artificial cerebrospinal fluid containing 300 μM NAS, and a progressive decline in the amplitude of the EPSC was subsequently observed over a 15 min period (Fig $1B_1$). This decline was largely an action of the applied drug because in a series of control cells recorded in the absence of NAS over the same time interval, the natural run down of the response was significantly slower (Fig $1B_2$). At 12 – 15 min, the response in NAS was reduced to 51 ± 17% of control. As a further demonstration that cell run down does not fully account for the decline in NAS, we observed partial recovery of the EPSC following washout of the drug (Fig. $1C_1$, $1C_2$). In NAS, the rise and decay times of the EPSCs were not significantly different from control (P > 0.05, t-test, n = 13), as expected for an open channel blocker.

Glutamate uncaging activates a polyamine-sensitive EPSC in ET cells

A second approach we took to analyze ET cell glutamate receptors was to evoke an EPSC by direct application of exogenous glutamate. Since this does not require activation of presynaptic terminals, voltage-gated Na^+ and Ca^{2+} conductances could be blocked by inclusion of TTX (1 μM) and Cd^{2+} (150 – 300 μM) in the bath solution. This allowed us to exclude contributions to the EPSC from the voltage-gated channels in finer branches of dendritic tufts, where voltage control may be difficult during large depolarizing currents. In trial experiments, we found that conventional agonist delivery methods such as glutamate iontophoresis or pressure ejection from puffer pipettes were relatively ineffective at stimulating ET cell dendrites. The reason for this may be that dendritic tufts are deeply embedded in the glomerular neuropil, perhaps enclosed in glial microcompartments (Kasowski et al., 1999). To overcome diffusion barriers, we employed flash photolysis of caged glutamate, a method capable of rapidly and efficiently activating AMPA receptors in olfactory bulb slices (Lowe, 2003). As in the olfactory nerve shock experiments, either dCK or APV were added to the bath to eliminate NMDA receptor currents and isolate the AMPA/kainate current.

Under whole-cell voltage-clamp (− 60 mV), flash photolysis of caged glutamate on ET cells activated large EPSCs with fast onset and slower decay kinetics. The magnitude of the responses depended on the uncaging light source, which determined the degree of photolysis. For N_2 laser uncaging, the amplitude was 265.3 ± 112.5 pA, the time to peak was 8.54 ± 2.05 ms, and the 50% decay time 48.03 ± 28.87 ms (n = 8); for the xenon flash lamp, the mean amplitude was 541.39 ± 86.64 pA, the rise time 6.01 ± 0.37 ms, and the 50% decay time 158.38 ± 50.65 ms (n = 34). These numbers describe initial data recorded within ~ 5 min of patch rupture, before whole cell dialysis caused rundown and slowing of responses. The greater mean amplitude and slower recovery of the responses evoked by flash lamp compared to the N_2 laser is consistent with the flash lamp having a wider illuminated area and higher estimated photolysis efficiency (see Methods). The slower mean rise time in the laser data can be explained if the smaller illuminated spot failed to precisely target dendritic receptor sites, incurring a glutamate diffusion delay. We analyzed the recovery kinetics of the cells stimulated by flash lamp uncaging. Of 34 cells, we found 25 that fit a double exponential decay consisting of the sum of a fast and a slow term, 5 that fit a single exponential decay (3 fast, 2 slow), and 4 that did not fit an exponential model. The mean time constants were 27.29 ± 5.30 ms for the fast decay (n = 28), and 746.4 ± 151.7 ms for the slow decay (n = 27). Amplitudes of the fast and slow terms were poorly correlated across the double exponential cells (R = 0.23), suggesting contributions from at least two independent currents. For example, the fast component might represent rapidly desensitizing AMPA receptors, and the slow component kainate receptors.

Addition of 100 μM cyclothiazide (CTZ), a selective modulator of AMPA receptor desensitization, strongly boosted the amplitude and duration of uncaging EPSCs (Fig. 2A). This showed that a substantial portion of the current was carried by AMPA receptors. Peak inward current in CTZ evoked by N_2 laser uncaging was 368.4 ± 126.4 pA (range 41.2 – 836.2 pA) (n = 8). Compared to control, CTZ amplified the peak laser-evoked currents by a factor of 1.85 ± 0.32, and extended 50% response recovery times by a factor of 5.87 ± 1.08 (n = 7). In CTZ, the mean EPSC time to peak was 14.1 ± 1.6 ms, and 50% decay time was 114 ± 29 ms (n = 11). The CTZ should also amplify spontaneous AMPA receptor currents, and indeed we sometimes observed heavy background synaptic activity in the presence of the drug (Fig. 2B). In most cells, background activity did not interfere with measurement of uncaging responses because CTZ-boosted spontaneous activity was lower (< 20 pA; Fig. 2A). The AMPA/kainate receptor antagonist NBQX fully abolished the uncaging responses recorded in either the presence or the absence of CTZ (n = 6).

To examine the contribution of calcium permeable AMPA receptors to the uncaging EPSC, we again challenged ET cells with the calcium permeable AMPA receptor antagonist NAS. These experiments were performed in 100 μm CTZ to magnify the AMPA receptor component. After introducing 300 μM NAS into the perfusion solution, we observed a progressive decline in the magnitude of the uncaging EPSC over 15 min, similar to the effect of the drug on the olfactory nerve shock-evoked EPSCs (Fig. 2C, 2D). These data were compared to the 15 min trend of the uncaging EPSC in a separate group of cells in the absence of NAS (Fig. 2D). This controlled for any intrinsic run down of the response that might have been caused by photodynamic damage due to repeated exposure to intense light flashes in the presence of fluorescent tracer dyes. We found that cells treated with NAS showed a significantly faster decline of the EPSC than the control group. At 12 – 15 min, the response in NAS was reduced to 49 ± 13% of control.

Inward rectification of the AMPA receptor EPSC

In intact neurons, current flowing through calcium permeable AMPA receptors is characterized by inward rectification. This occurs because, at positive membrane potentials, endogenous cytoplasmic polyamines can plug the channel pore, attenuating the outward current (Donevan and Rogawski, 1995). An inwardly rectifying EPSC would be further evidence for calcium permeable AMPA receptors, so we have examined the current-voltage (I-V) relation of the uncaging EPSC in ET cells. Fig. 3A shows an I-V curve obtained from an ET cell in which we detected weak inward rectification at the beginning of whole-cell recording (≤ 5 min after patch rupture). After ≥ 10 min of whole cell recording, the inward rectification disappeared. This loss occurred consistently in a sample of 6 cells. The rectification index (RI) increased from 0.76 ± 0.08 to 1.4 ± 0.4 ($P < 0.05$), with 2 of 6 cells transitioning to outward rectification (Fig. 3C). Dialysis of soluble factors from the dendrites, such as polyamines, might explain loss of inward rectification over time. To test this, we recorded from cells using an internal solution augmented with 75 – 250 μM spermine, a polyamine that blocks calcium permeable AMPA channels. However, this failed to prevent loss of rectification (RI increased from 0.74 ± 0.08 to 1.25 ± 0.17, $P < 0.05$, $n = 13$ cells), perhaps because diffusion barriers hindered the loading of spermine from the pipette into the dendritic tuft. The same diffusion barrier might arguably have hindered washout of endogenous polyamines and loss of inward rectification. However the identity and native concentrations of these substances in the dendrites effective for channel block is unknown. As a second test, we measured I-V curves of the uncaging EPSC with 300 μM NAS present in the bath. We found that NAS eliminated the initial inward rectification of current, consistent with calcium permeable AMPA receptors being the source of the rectification (RI = 0.91 ± 0.08 ≤ 5 min, 0.98 ± 0.09 ≥ 10 min, $n = 7$) (Fig B). Reversal potential in NAS (14.3 ± 3.5 mV, $n = 7$) was not significantly different from controls (11.3 ± 4.4 mV, $n = 6$; $P > 0.05$). Could the action of NAS be due to non-specific deleterious effects on cell condition, unrelated to specific block of calcium permeable AMPA receptors? This could happen for example if NAS accelerated loss of internal rectifying factors from the dendrites simply by making the membrane leaky. We excluded this possibility by tracking the change in whole-cell input resistance as NAS was washed into the bath. Over a 20 min period of recording, there was no significant difference between the input resistances of cells exposed to 300 μM NAS and control cells (Fig 3D).

Calcium transients associated with the AMPA receptor EPSC

To obtain more direct evidence that ET cells express calcium permeable AMPA receptors, we sought to detect Ca^{2+} influx through these receptors directly by fluorometry. Our strategy was to activate AMPA receptors by uncaging glutamate onto the cell, and measure intracellular Ca^{2+} while blocking alternative routes of Ca^{2+} entry. Voltage-sensitive Ca^{2+} channels were blocked with Cd^{2+} (150 – 200 μM), and NMDA receptors with dCK (15 μM), and the AMPA receptor EPSC was amplified and prolonged using 100 μM CTZ. Glutamate was uncaged by

focusing an argon ion laser in the vicinity of the soma and proximal dendrite, and fluorescence emission collected by a photodiode. The photodiode spatially summated the Ca^{2+} signal over an extended region of the cell including the soma and proximal dendrite. Under these conditions, the high affinity calcium indicator fluo-4 could detect fluorescence transients occurring in parallel with large uncaging EPSCs (Fig. 4C) in 8 of 15 recorded ET cells. The relative fluorescence change, $\Delta F/F_0$, had a peak amplitude of 1.4 – 5.1%, a mean time to peak of 148 ± 20 ms (n = 8), and was positively correlated with the EPSC amplitude (R = 0.76) (Fig. 4F). The time course of $\Delta F/F_0$ did not simply track the integrated charge transfer, but attained a plateau level which could represent either indicator saturation or competitive Ca^{2+} binding by a high affinity buffer inside the cell (Fig. 4D). We considered if the fluorescence signal was derived not from Ca^{2+} permeable AMPA/kainate receptors, but from voltage-sensitive Ca^{2+} channels that were not blocked by Cd^{2+}. Although we expected good voltage clamp to be maintained at the soma and proximal dendrite where the uncaging spot was focused, glutamate may have diffused to finer distal dendritic branches and activated local inward currents that escaped voltage clamp. Such depolarization could have activated Cd^{2+} -resistant low threshold Ca^{2+} channels responsible for generating plateau potentials during ET cell burst firing (Zhou et al., 2006). However, we could still detect fluorescence transients in the presence of 250 μM Ni^{2+}, which blocks low threshold channels (n = 4). Moreover, voltage pulse depolarizations (−60 to 0 mV, 50 ms) failed to evoke Ca^{2+} transients, even though they should have opened voltage-sensitive Ca^{2+} channels (n = 3) (Fig. 4E). We also noted that the combination of 150 μM Cd^{2+} and 250 μM Ni^{2+} eliminated any measurable Ca^{2+} current in ET cells (Fig. 4B). Another alternative is that the glutamate-evoked Ca^{2+} transient might be mediated by metabotropic glutamate receptor 1 (mGluR1). In mitral cells, mGluR1 is responsible for the genesis of a slow potential and accompanying Ca^{2+} transient in the apical dendritic tuft (Yuan and Knopfel, 2006). There is strong mGluR1 immunoreactivity in glomeruli (Sahara et al., 2001), and the receptor is expressed in a subset of juxtaglomerular neurons which could include ET cells (Heinbockel et al., 2004). However, we found that uncaging glutamate could elicit the fluorescence signal in ET cells even in the presence of 1 mM (+)-MCPG ($\Delta F/F_0$ = 1.4 – 3.2%, n = 2), an mGluR1 antagonist that blocks the mitral cell tuft Ca^{2+} transient (Yuan and Knopfel, 2006).

Kainate stimulates Co^{2+} entry into cells of the glomerular layer

A well documented property of the calcium permeable AMPA receptor is its ability to permeate to cobalt ions (Pruss et al., 1991). In the presence of cobalt, we stimulated slices by perfusion with kainate, a non-desensitizing agonist of ionotropic glutamate receptors. Activation of NMDA receptors was blocked by 100 μM APV and 100 μM dCK. Strong cobalt staining, visualized in 0.12% $(NH_4)_2S$, was observed in the glomerular layer of kainate exposed slices, including punctuate labeling of somata near the external plexiform layer where ET cells reside (Fig. 5A, 5B). Cobalt staining was not observed in two control conditions: slices were exposed to cobalt without kainate (Fig. 5C, D), and slices were exposed to cobalt and kainate, in the presence of the AMPA/kainate receptor antagonist NBQX (100 μM) (Fig. 5E, 5F). Similar data were obtained from 3 rats, using 2 olfactory bulb slices for each condition (stimulus and two controls). These data confirm results obtained from juxtaglomerular cells in another recent study (Blakemore et al., 2006), and they provide further support for the expression of calcium permeable AMPA receptors in neurons of the glomerular layer.

Depolarization activates a polyamine-sensitive AMPA receptor current

In the olfactory bulb, glutamate released from dendrites of a mitral cell can activate receptors on the same cell, leading to self-excitation (Nicoll and Jahr, 1982; Friedman and Strowbridge, 2000; Salin et al., 2001). Mitral cells express both AMPA and NMDA types of glutamate autoreceptors (Margrie et al., 2001). The AMPA autoreceptors are of special interest in that they appear to play a central role in maintaining spike synchronization among pairs of mitral

cells with shared glomerular projections (Schoppa and Westbrook, 2002; Christie et al., 2005). Like the mitral cells, ET cells are principal neurons, and their burst firing is synchronized when they project their dendritic tufts into the same glomerulus. Do they also express AMPA autoreceptors? If so, might they be calcium permeable? To investigate this, we applied depolarizing voltage-pulses to ET cells to evoke dendritic transmitter release and looked for signs of recurrent excitation.

In these experiments, we blocked voltage-gated Na^+ and K^+ channels, as well as NMDA receptors, and used CTZ to amplify any currents arising from AMPA receptors. We still permitted voltage-sensitive Ca^{2+} channels to open, so they could drive transmitter release. Fig. 6A shows typical data recorded from an ET cell in which a voltage step from − 60 mV to 0 mV activated a Ca^{2+} current, and upon repolarization a substantial 'tail' current was observed. This tail current was largely abolished by 10 μM NBQX, confirming that it mostly originated from AMPA/kainate receptors (charge transfer in NBQX was 2.2 – 23% of control, in a sample of 10 cells). To quantify the AMPA/kainate part of the current, we integrated the total charge transfer and subtracted from it the integral of the tail current in NBQX which should comprise the sum of the capacitance and residual Ca^{2+} channel tail currents (charge in NBQX, 2.4 ± 0.3 pC, $n = 10$). The mean AMPA/kainate charge transfer estimated this way was 34 ± 6 pC (range 13.2 – 64.8 pC; $n = 10$). The tail current appeared to depend on glutamate release from the recorded cell, because it was stabilized by dialysis of glutamate (30 mM) from the whole-cell pipette. When glutamate was omitted from the internal solution, we could still record a large initial tail current (charge transfers 16, 40 and 334 pC; $n = 3$ cells), but the response decayed sharply with repeated stimulation and was lost after > 6 trials. Thus, the tail current was not just an artefact of glutamate loading from the pipette,

We next analyzed the effect of the calcium permeable AMPA receptor antagonist NAS on the tail current. Perfusion of cells with 300 μM NAS resulted in a major attenuation of the AMPA/kainate current, with charge transfer reduced to 16 ± 4% of control ($n = 8$). In a second group of cells which did not survive sufficiently long to perform a measurement in NBQX, the addition of NAS also strongly reduced the raw charge transfer, to 30 ± 7% of control ($n = 5$). Since CTZ amplification is specific for AMPA receptors, strong attenuation by NAS indicates that much of the tail current is contributed by calcium permeable AMPA receptors. Indeed, the addition of CTZ boosted the charge transfer by a factor of 2.4 – 12.7 (mean ratio 7.6 ± 1.4, $n = 6$).

The large drop in charge transfer following the switch to NAS perfusion was not due to rundown of the tail current responses because, in a control group of 7 cells, the average charge transfer was still at 93 ± 30% of the initial value after recording for 30 min, the maximum time period for NAS perfusion. This assertion receives further support from partial recovery of the tail current (79 ± 15%, $n = 9$) after washout of the drug (Fig. 6B, 6C). We also considered the possibility that NAS could attenuate the tail current indirectly, by non-specific antagonism of Ca^{2+} channels responsible for transmitter release. To test this, we derived a partial measure of Ca^{2+} channel charge transfer by integrating the net inward current during the 100 ms voltage-pulse, referenced to the current value immediately prior to stepping back to − 60 mV. During this time interval, the membrane was clamped at 0 mV, so any AMPA receptors already open should be near their reversal potential, and the current should be dominated by Ca^{2+} channels. In contrast to the tail current, we found that the Ca^{2+} channel charge transfer was not significantly attenuated by NAS (Fig. 6C). We therefore concluded that NAS was most likely to be acting directly on the AMPA receptors, in agreement with our results from the uncaging of glutamate. If in fact the tail current is an autoreceptor current caused by transmitter release, then it should be abolished by blocking Ca^{2+} channels. This we confirmed by applying 300 μM Cd^{2+} to the bath, which abolished the tail current in CTZ, leaving only a whole-cell capacitance transient (charge 4.9 ± 2.6 pC, $n = 4$). To quantify the NAS-sensitive component

of the tail current, we subtracted the current in NAS from the pre-NAS control current (Fig. 1A). The mean subtracted amplitude was 181 ± 30 pA (range 85 – 408 pA), charge transfer was 21.8 ± 3.5 pC (range 5 – 48 pC), and 50% decay time was 116 ± 19 ms (range 43 – 273 ms). Since these measurements were made in CTZ, this slow decay likely represents the kinetics of glutamate release and diffusion, rather than receptor desensitization.

Glutamate release from ET cells activates an autoreceptor

To demonstrate that transmitter released from ET cells actually activates autoreceptors, we must exclude a multi-neuronal origin for the AMPA receptor tail current. Since mitral cells and perhaps ET cells in the same glomerulus could mutually excite each another by gap junctions or glutamate spillover (Schoppa and Westbrook, 2002; Urban and Sakmann, 2002; Hayar et al., 2005; Christie and Westbrook, 2006), depolarizing one ET cell may activate adjacent ET or mitral cells, leading to recurrent glutamatergic excitation. To resolve these ambiguities, we triggered glutamate release from ET cells by uncaging intracellular calcium. This method enabled us to maintain voltage clamp at − 60 mV (which prevented depolarization of electrically coupled neurons), and to block Ca^{2+} entry with 500 μM Cd^{2+} (which prevented high threshold Ca^{2+} channel-mediated glutamate release from neighboring neurons). Cells were dialyzed with 5 mM or 10 mM DM-nitrophen, 60% loaded with bound $CaCl_2$, and calcium was uncaged by a xenon flash lamp. We first omitted CTZ from the bath to allow AMPA receptors to desensitize normally and limit spillover transmission to physiologically effective distances. Under these conditions, flash photolysis evoked large, transient inward currents. The mean current amplitude was 350 ± 90 pA (range 19 – 1344 pA), rise time was 5.9 ± 0.9 ms (range 0.42 – 15.9 ms), and 50% decay time was 10.9 ± 1.9 ms (range 1.1 – 33.4 ms) (n = 17 cells). In some experiments, we removed Ca^{2+} from the bath solution and were still able to record large flash responses (n = 3). This makes it unlikely that there was recurrent transmitter release from adjacent excited cells mediated by Cd^{2+} resistant Ca^{2+} channels. We excluded a role for low threshold Ca^{2+} channels in recurrent excitatory transmission because perfusion with 250 μM Ni^{2+} did not block the photolysis-evoked currents (n = 2 cells, in CTZ). These currents had a fast onset, with no measurable latency, and a fast rise time, which argues against multi-neuronal spillover transmission. Although we were unable to conduct pharmacological analyses of flash responses in individual cells because of their instability over time, we propose to interpret them as AMPA autoreceptor currents because: (i) uncaging calcium in ET cells releases glutamate, as indicated by dendrodendritic feedback inhibition (Murphy et al., 2005); (ii) NMDA receptors were blocked, (iii) the fast kinetics were typical of AMPA receptors; and (iv) when CTZ was present, flash responses were significantly prolonged compared to the non-CTZ group (P = 0.0004), with 50% decay times of 75 ± 28 ms (n = 6).

DISCUSSION

We present several lines of evidence to support the hypothesis that functional calcium permeable AMPA receptors are expressed in ET cells. First, we show that application of the calcium permeable AMPA receptor selective antagonist NAS to olfactory bulb slices significantly attenuated (~ 50%) both the EPSC and the autoreceptor current in ET cells. The concentration of NAS that was effective (300 μM) was higher than that employed in some investigations of other cells, for example in cultured hippocampal neurons (3 μM) (Koike et al., 1997), motoneurons (5 – 10 μM) (Van Damme et al., 2002) or NG2 cells in hippocampal slices (30 – 50 μM) (Ge et al., 2006). However, 300 μM NAS was required to block Co^{2+} and Zn^{2+} entry into hippocampal neurons in slices and in culture (Yin et al., 2002; Ogoshi and Weiss, 2003), and it was also used to block currents in excised patches (Jia et al., 2002). In the olfactory bulb, Blakemore et al. (2006) reported that 10 μM NAS was sufficient to attenuate the olfactory nerve shock-evoked EPSC in a sample of juxtaglomerular cells, which might have included ET cells. In our hands, 100 μM bath perfusion did not appreciably diminish the mean

EPSC amplitude of ET cells relative to a group of control cells. We suggest that these apparent differences in efficacy could be a function of the structural integrity of slice preparations, and the extent of encapsulation of ET cell dendritic tufts within glial compartments of olfactory glomeruli. Since we tried to target ET somata located well below the surface of the slice to avoid selection of injured neurons, their dendrites were more likely to be deeply entrenched in the glomerular neuropil. This may have retarded access of bath-applied NAS to postsynaptic receptors. A similar degree of EPSC attenuation was seen in both olfactory nerve-shock and glutamate uncaging experiments, so it is unlikely that the inhibitory action of NAS was caused by non-specific antagonism of transmitter release machinery.

In the presence of polyamines, calcium permeable AMPA/kainate receptor-mediated currents elicited by repeated agonist challenges can experience a progressive use-dependent blockade (Koike et al., 1997; Bowie et al., 1998). This is a characteristic of open channel blockers. We did see an initial stepwise decrement of the EPSC amplitude during repeated ET cell stimulation in NAS over a 15 min period. However, the complex environment of the slice makes it difficult to interpret this fall off as a simple use-dependent block determined only by the number of stimulations. We expect additional complications to arise from a non-steady concentration of NAS at the receptor sites, due to delayed penetration into the glomerulus, and a continuous use-dependent block associated with ongoing spontaneous excitatory synaptic activity (Figs. 1A, 2B).

A second property of calcium permeable AMPA receptors that we examined was inward rectification of the I-V curve. We found significant inward rectification (RI < 1) in glutamate-evoked EPSCs at the start of whole-cell recording, and this was lost during the course of the experiment, as if endogenous channel-blocking factors were being dialyzed from the dendrites. The lack of inward rectification (RI ~ 1) in the presence of NAS is consistent with a role for calcium permeable AMPA receptors. It is unclear why inclusion of spermine in the internal solution pipette did not prevent loss of rectification. The rate of loading of spermine from the pipette into the finer branches of the dendritic tuft may have been insufficient to counteract a drop in locally high levels of endogenous polyamines during whole cell dialysis.

The third, most direct evidence for calcium permeable AMPA receptors in ET cells was fluorometric detection of calcium entry during activation of a CTZ-enhanced AMPA receptor EPSC by uncaged glutamate. Calcium entry through other conductances (NMDA receptors or voltage-sensitive Ca^{2+} channels) was excluded pharmacologically, or by voltage-clamp control experiments. A fourth line of evidence is the labeling of juxtaglomerular neurons by cobalt uptake, which is selective for calcium permeable AMPA and not kainate receptors (Malva et al., 2003). This finding was first reported by Blakemore et al 2006, and we are in agreement with their result.

The role of calcium permeable AMPA receptors in normal olfactory processing remains to be determined. In transgenic mice with either depleted expression of the GluR2 subunit, or expression of unedited GluR2 in forebrain and olfactory bulb, odor discrimination and learning are enhanced but olfactory memory is impaired (Shimshek et al., 2005). Memory performance alone could be rescued by localized expression of GluR2 in hippocampus and piriform cortex, so it was inferred that the effects on discrimination and learning were likely to be specific to the olfactory bulb. This suggests that, in principle, modulation of AMPA receptor calcium permeability in the bulb can strongly impact olfactory function. For instance, upregulation of the number of calcium permeable AMPA receptors at dendrodendritic synapses would selectively augment Ca^{2+} entry and amplify lateral or feedback inhibitory transmission in glomerular or mitral-granule circuits associated with specific olfactory receptors.

In ET cells, our data suggest the presence of at least two segregated pools of calcium permeable AMPA receptors – postsynaptic receptors at axodendritic olfactory nerve synapses, and autoreceptors associated with dendritic glutamate release sites. What can these receptors contribute to normal ET cell function? It has been proposed that the role of olfactory nerve synaptic input is to entrain the pacemaker-like burst firing of a population of ET cells, keeping it time-locked to the sniff cycle during odorant sampling (Hayar et al., 2004b). Synchronously bursting ET cells are envisaged to coordinate the timing of olfactory processing in glomerular circuits through periglomerular cell-mediated inhibition, for example by imposing a temporal window on sensory integration by mitral and tufted cells, and lateral inhibition by short axon cells (Wachowiak and Shipley, 2006). A postsynaptic calcium signal offers a readout option for integrating and recording the recent history of sensory input to olfactory bulb neurons. The calcium permeable AMPA receptors have particularly rapid kinetics (Li et al., 2003), so they are well suited to the task of encoding synaptic input as a dendritic calcium signal over a broad frequency band. Calcium influx through AMPA receptors can be involved in long term potentiation (Jia et al., 1996; Mahanty and Sah, 1998; Feldmeyer et al., 1999) or long term depression (Soler-Llavina and Sabatini, 2006), independent of NMDA-receptors. Calcium dependent induction of synaptic plasticity has been proposed in models of conditioned olfactory learning (Yuan et al., 2003). Calcium entry via NMDA receptors is a well known step in long term potentiation at various synapses. Unlike NMDA receptors, whose voltage-dependent Mg^{2+} block inhibits Ca^{2+} entry unless the membrane is depolarized, the calcium permeable AMPA receptors can operate as linear calcium encoders across a wide range of voltages. Hence they would faithfully register and encode sensory input at any phase of ET cell firing, regardless of the timing of action potential bursts relative to synaptic input. An experience-dependent modulation of olfactory nerve-ET synaptic strength might be part of an early olfactory learning mechanism that regulates the sensitivity of specific glomeruli to odorant stimuli.

The AMPA autoreceptors on ET cells might serve a purpose similar to the role played by AMPA autoreceptors on mitral cell dendritic tufts (Schoppa and Westbrook, 2002; Christie et al., 2005). If they generate a slow post-burst depolarization, this could be relayed to other ET cells in the same glomerulus by dendrodendritic electrical couplings, thereby assisting the establishment of burst synchrony (Hayar et al., 2005). Although it may seem that a slow plateau potential generated by low threshold Ca^{2+} channels should dominate any AMPA autoreceptor potential (McQuiston and Katz, 2001), the plateau potential has a refractory period that limits its activation to bursting frequencies below about 2.6 Hz (Zhou et al., 2006). An autoreceptor potential may become more important as ET cells are entrained by higher frequency sniffing up to 10 Hz (Hayar et al., 2004b). The calcium permeability of the AMPA autoreceptors suggests that they could perform other functions. The absence of any measurable latency in the caged Ca^{2+} currents implies that at least some autoreceptors reside in close proximity to the transmitter release sites on the ET cell dendrite. If calcium ions entering the cell through these autoreceptors formed local microdomains of high Ca^{2+} (Goldberg et al., 2003; Soler-Llavina and Sabatini, 2006), either overlapping or within diffusion range of Ca^{2+} sensors of the dendritic release machinery, it would complete a positive feedback loop capable of amplifying glutamate release. We speculate that this may constitute an ‘avalanche’ mode of neurotransmission, that might be advantageous for controlling the sensitivity and gain of dendrodendritic signaling. It could selectively amplify synaptic output from action potential bursts over spurious action potentials generated by noisy synaptic input from sensory neurons.

Acknowledgements

We gratefully acknowledge critical review of this manuscript by A. Gelperin and A. Ghatpande. This research was supported by a grant from NIDCD (DC04208).

References

Ajima A, Hensch T, Kado RT, Ito M. Differential blocking action of Joro spider toxin analog on parallel fiber and climbing fiber synapses in cerebellar Purkinje cells. Neurosci Res 1991;12:281–286. [PubMed: 1684239]

Antal M, Eyre M, Finklea B, Nusser Z. External tufted cells in the main olfactory bulb form two distinct subpopulations. Eur J Neurosci 2006;24:1124–1136. [PubMed: 16930438]

Aroniadou-Anderjaska V, Ennis M, Shipley MT. Glomerular synaptic responses to olfactory nerve input in rat olfactory bulb slices. Neuroscience 1997;79:425–434. [PubMed: 9200726]

Asami T, Kagechika H, Hashimoto Y, Shudo K, Miwa A, Kawai N, Nakajima T. Acylpolyamines mimic the action of joro spider toxin (JSTX) on crustacean muscle glutamate receptors. Biomed Res 1989;10:185–189.

Aungst JL, Heyward PM, Puche AC, Karnup SV, Hayar A, Szabo G, Shipley MT. Centre-surround inhibition among olfactory bulb glomeruli. Nature 2003;426:623–629. [PubMed: 14668854]

Barry PH. JPCalc, a software package for calculating liquid junction potential corrections in patch-clamp, intracellular, epithelial and bilayer measurements and for correcting junction potential measurements. J Neurosci Methods 1994;51:107–116. [PubMed: 8189746]

Berkowicz DA, Trombley PQ, Shepherd GM. Evidence for glutamate as the olfactory receptor cell neurotransmitter. J Neurophysiol 1994;71:2557–2561. [PubMed: 7931535]

Blakemore LJ, Resasco M, Mercado MA, Trombley PQ. Evidence for Ca(2+)-permeable AMPA receptors in the olfactory bulb. Am J Physiol Cell Physiol 2006;290:C925–C935. [PubMed: 16267106]

Blakemore LJ, Trombley PQ. Kinetic variability of AMPA receptors among olfactory bulb neurons in culture. Neuroreport 2003;14:965–970. [PubMed: 12802184]

Bowie D, Lange GD, Mayer ML. Activity-dependent modulation of glutamate receptors by polyamines. J Neurosci 1998;18:8175–8185. [PubMed: 9763464]

Christie JM, Bark C, Hormuzdi SG, Helbig I, Monyer H, Westbrook GL. Connexin36 mediates spike synchrony in olfactory bulb glomeruli. Neuron 2005;46:761–772. [PubMed: 15924862]

Christie JM, Westbrook GL. Lateral excitation within the olfactory bulb. J Neurosci 2006;26:2269–2277. [PubMed: 16495454]

Dingledine R, Borges K, Bowie D, Traynelis SF. The glutamate receptor ion channels. Pharmacol Rev 1999;51:7–61. [PubMed: 10049997]

Donevan SD, Rogawski MA. Intracellular polyamines mediate inward rectification of Ca^{2+}-permeable alpha-amino-3-hydroxy-5-methyl-4-isoxazolepropionic acid receptors. Proc Natl Acad Sci U S A 1995;92:9298–9302. [PubMed: 7568121]

Edwards JG, Michel WC. Pharmacological characterization of ionotropic glutamate receptors in the zebrafish olfactory bulb. Neuroscience 2003;122:1037–1047. [PubMed: 14643770]

Egebjerg J, Heinemann SF. Ca^{2+} permeability of unedited and edited versions of the kainate selective glutamate receptor GluR6. Proc Natl Acad Sci U S A 1993;90:755–759. [PubMed: 7678465]

Ennis M, Zimmer LA, Shipley MT. Olfactory nerve stimulation activates rat mitral cells via NMDA and non- NMDA receptors in vitro. Neuroreport 1996;7:989–992. [PubMed: 8804037]

Feldmeyer D, Kask K, Brusa R, Kornau HC, Kolhekar R, Rozov A, Burnashev N, Jensen V, Hvalby O, Sprengel R, Seeburg PH. Neurological dysfunctions in mice expressing different levels of the Q/R site-unedited AMPAR subunit GluR-B. Nat Neurosci 1999;2:57–64. [PubMed: 10195181]

Friedman D, Strowbridge BW. Functional role of NMDA autoreceptors in olfactory mitral cells. J Neurophysiol 2000;84:39–50. [PubMed: 10899181]

Ge WP, Yang XJ, Zhang Z, Wang HK, Shen W, Deng QD, Duan S. Long-term potentiation of neuron-glia synapses mediated by Ca^{2+}-permeable AMPA receptors. Science 2006;312:1533–1537. [PubMed: 16763153]

Giustetto M, Bovolin P, Fasolo A, Bonino M, Cantino D, Sassoe-Pognetto M. Glutamate receptors in the olfactory bulb synaptic circuitry: heterogeneity and synaptic localization of N-methyl-D-aspartate receptor subunit 1 and AMPA receptor subunit 1. Neuroscience 1997;76:787–798. [PubMed: 9135051]

Goldberg JH, Tamas G, Aronov D, Yuste R. Calcium microdomains in aspiny dendrites. Neuron 2003;40:807–821. [PubMed: 14622584]

Hayar A, Karnup S, Ennis M, Shipley MT. External tufted cells: a major excitatory element that coordinates glomerular activity. J Neurosci 2004a;24:6676–6685. [PubMed: 15282270]

Hayar A, Karnup S, Shipley MT, Ennis M. Olfactory bulb glomeruli: external tufted cells intrinsically burst at theta frequency and are entrained by patterned olfactory input. J Neurosci 2004b;24:1190–1199. [PubMed: 14762137]

Hayar A, Shipley MT, Ennis M. Olfactory bulb external tufted cells are synchronized by multiple intraglomerular mechanisms. J Neurosci 2005;25:8197–8208. [PubMed: 16148227]

Heinbockel T, Heyward P, Conquet F, Ennis M. Regulation of main olfactory bulb mitral cell excitability by metabotropic glutamate receptor mGluR1. J Neurophysiol 2004;92:3085–3096. [PubMed: 15212418]

Horning MS, Kwon B, Blakemore LJ, Spencer CM, Goltz M, Houpt TA, Trombley PQ. Alpha-amino-3-hydroxy-5-methyl-4-isoxazolepropionate receptor subunit expression in rat olfactory bulb. Neurosci Lett 2004;372:230–234. [PubMed: 15542246]

Hume RI, Dingledine R, Heinemann SF. Identification of a site in glutamate receptor subunits that controls calcium permeability. Science 1991;253:1028–1031. [PubMed: 1653450]

Isaac JT, Wheal HV. The local anaesthetic QX-314 enables enhanced whole-cell recordings of excitatory synaptic currents in rat hippocampal slices in vitro. Neurosci Lett 1993;150:227–230. [PubMed: 8385755]

Jia Y, Jeng JM, Sensi SL, Weiss JH. Zn^{2+} currents are mediated by calcium-permeable AMPA/kainate channels in cultured murine hippocampal neurones. J Physiol 2002;543:35–48. [PubMed: 12181280]

Jia Z, Agopyan N, Miu P, Xiong Z, Henderson J, Gerlai R, Taverna FA, Velumian A, MacDonald J, Carlen P, Abramow-Newerly W, Roder J. Enhanced LTP in mice deficient in the AMPA receptor GluR2. Neuron 1996;17:945–956. [PubMed: 8938126]

Kasowski HJ, Kim H, Greer CA. Compartmental organization of the olfactory bulb glomerulus. J Comp Neurol 1999;407:261–274. [PubMed: 10213094]

Keller A, Yagodin S, Aroniadou-Anderjaska V, Zimmer LA, Ennis M, Sheppard NFJ, Shipley MT. Functional organization of rat olfactory bulb glomeruli revealed by optical imaging. J Neurosci 1998;18:2602–2612. [PubMed: 9502819]

Koike M, Iino M, Ozawa S. Blocking effect of 1-naphthyl acetyl spermine on Ca^{2+}-permeable AMPA receptors in cultured rat hippocampal neurons. Neurosci Res 1997;29:27–36. [PubMed: 9293490]

Li G, Pei W, Niu L. Channel-opening kinetics of GluR2Q(flip) AMPA receptor: a laser-pulse photolysis study. Biochemistry 2003;42:12358–12366. [PubMed: 14567697]

Lowe G. Inhibition of backpropagating action potentials in mitral cell secondary dendrites. J Neurophysiol 2002;88:64–85. [PubMed: 12091533]

Lowe G. Flash photolysis reveals a diversity of ionotropic glutamate receptors on the mitral cell somatodendritic membrane. J Neurophysiol 2003;90:1737–1746. [PubMed: 12724365]

Ma J, Lowe G. Action potential backpropagation and multiglomerular signaling in the rat vomeronasal system. J Neurosci 2004;24:9341–9352. [PubMed: 15496670]

Mahanty NK, Sah P. Calcium-permeable AMPA receptors mediate long-term potentiation in interneurons in the amygdala. Nature 1998;394:683–687. [PubMed: 9716132]

Malva JO, Vieira AP, Ambrosio AF, Oliveira CR. Cobalt staining of hippocampal neurons mediated by non-desensitizing activation of AMPA but not kainate receptors. Neuroreport 2003;14:847–850. [PubMed: 12858045]

Margrie TW, Sakmann B, Urban NN. Action potential propagation in mitral cell lateral dendrites is decremental and controls recurrent and lateral inhibition in the mammalian olfactory bulb. Proc Natl Acad Sci U S A 2001;98:319–324. [PubMed: 11120888]

McQuiston AR, Katz LC. Electrophysiology of interneurons in the glomerular layer of the rat olfactory bulb. J Neurophysiol 2001;86:1899–1907. [PubMed: 11600649]

Mombaerts P, Wang F, Dulac C, Chao SK, Nemes A, Mendelsohn M, Edmondson J, Axel R. Visualizing an olfactory sensory map. Cell 1996;87:675–686. [PubMed: 8929536]

Montague AA, Greer CA. Differential distribution of ionotropic glutamate receptor subunits in the rat olfactory bulb. J Comp Neurol 1999;405:233–246. [PubMed: 10023812]

Murphy GJ, Darcy DP, Isaacson JS. Intraglomerular inhibition: signaling mechanisms of an olfactory microcircuit. Nat Neurosci. 2005

Murphy GJ, Glickfeld LL, Balsen Z, Isaacson JS. Sensory neuron signaling to the brain: properties of transmitter release from olfactory nerve terminals. J Neurosci 2004;24:3023–3030. [PubMed: 15044541]

Nicoll RA, Jahr CE. Self-excitation of olfactory bulb neurones. Nature 1982;296:441–444. [PubMed: 6278326]

Ogoshi F, Weiss JH. Heterogeneity of Ca^{2+}-permeable AMPA/kainate channel expression in hippocampal pyramidal neurons: fluorescence imaging and immunocytochemical assessment. J Neurosci 2003;23:10521–10530. [PubMed: 14627636]

Ozawa S, Kamiya H, Tsuzuki K. Glutamate receptors in the mammalian central nervous system. Prog Neurobiol 1998;54:581–618. [PubMed: 9550192]

Pinching AJ, Powell TP. The neuron types of the glomerular layer of the olfactory bulb. J Cell Sci 1971;9:305–345. [PubMed: 4108056]

Pruss RM, Akeson RL, Racke MM, Wilburn JL. Agonist-activated cobalt uptake identifies divalent cation-permeable kainate receptors on neurons and glial cells. Neuron 1991;7:509–518. [PubMed: 1716930]

Sahara Y, Kubota T, Ichikawa M. Cellular localization of metabotropic glutamate receptors mGluR1, 2/3, 5 and 7 in the main and accessory olfactory bulb of the rat. Neurosci Lett 2001;312:59–62. [PubMed: 11595334]

Salin PA, Lledo PM, Vincent JD, Charpak S. Dendritic glutamate autoreceptors modulate signal processing in rat mitral cells. J Neurophysiol 2001;85:1275–1282. [PubMed: 11247996]

Sassoe-Pognetto M, Utvik JK, Camoletto P, Watanabe M, Stephenson FA, Bredt DS, Ottersen OP. Organization of postsynaptic density proteins and glutamate receptors in axodendritic and dendrodendritic synapses of the rat olfactory bulb. J Comp Neurol 2003;463:237–248. [PubMed: 12820158]

Schoppa NE, Westbrook GL. AMPA autoreceptors drive correlated spiking in olfactory bulb glomeruli. Nat Neurosci 2002;5:1194–1202. [PubMed: 12379859]

Shimshek DR, Bus T, Kim J, Mihaljevic A, Mack V, Seeburg PH, Sprengel R, Schaefer AT. Enhanced odor discrimination and impaired olfactory memory by spatially controlled switch of AMPA receptors. PLoS Biol 2005;3:e354. [PubMed: 16216087]

Soler-Llavina GJ, Sabatini BL. Synapse-specific plasticity and compartmentalized signaling in cerebellar stellate cells. Nat Neurosci 2006;9:798–806. [PubMed: 16680164]

Trombley PQ, Shepherd GM. Synaptic transmission and modulation in the olfactory bulb. Curr Opin Neurobiol 1993;3:540–547. [PubMed: 8219719]

Urban NN, Sakmann B. Reciprocal intraglomerular excitation and intra- and interglomerular lateral inhibition between mouse olfactory bulb mitral cells. J Physiol 2002;542:355–367. [PubMed: 12122137]

Van Damme P, Van Den BL, Van Houtte E, Callewaert G, Robberecht W. GluR2-dependent properties of AMPA receptors determine the selective vulnerability of motor neurons to excitotoxicity. J Neurophysiol 2002;88:1279–1287. [PubMed: 12205149]

Wachowiak M, Shipley MT. Coding and synaptic processing of sensory information in the glomerular layer of the olfactory bulb. Semin Cell Dev Biol. 2006

Yin HZ, Sensi SL, Ogoshi F, Weiss JH. Blockade of Ca^{2+}-permeable AMPA/kainate channels decreases oxygen-glucose deprivation-induced Zn^{2+} accumulation and neuronal loss in hippocampal pyramidal neurons. J Neurosci 2002;22:1273–1279. [PubMed: 11850455]

Yuan Q, Harley CW, Darby-King A, Neve RL, McLean JH. Early odor preference learning in the rat: bidirectional effects of cAMP response element-binding protein (CREB) and mutant CREB support a causal role for phosphorylated CREB. J Neurosci 2003;23:4760–4765. [PubMed: 12805315]

Yuan Q, Knopfel T. Olfactory nerve stimulation-evoked mGluR1 slow potentials, oscillations, and calcium signaling in mouse olfactory bulb mitral cells. J Neurophysiol 2006;95:3097–3104. [PubMed: 16467433]

Zhou Z, Xiong W, Masurkar AV, Chen WR, Shepherd GM. Dendritic Calcium Plateau Potentials Modulate Input-Output Properties of Juxtaglomerular Cells in the Rat Olfactory Bulb. J Neurophysiol 2006;96:2354–63. [PubMed: 16855116]

List of Abbreviations

AMPA
alpha-amino-3-hydroxy-5-methyl-4-isoxazolepropionic acid

CTZ
cyclothiazide

dCK
5,7-dichlorokynurenic acid

EPL
external plexiform layer

EPSC
excitatory postsynaptic current

ET
external tufted

GABA
gamma-aminobutyric acid

GCL
granule cell layer

GL
glomerular layer

HEPES
4-(2-hydroxyethyl)-1-piperazineethanesulfonic acid

KA
kainate

MCPG
(+)-α-Methyl-4-carboxyphenylglycine

mGluR1
metabotropic glutamate receptor 1

MNI
4-methoxy-7-nitroindolinyl

NAS
1-naphthyl acetyl-spermine

NBQX
(±)-4-(4-Aminophenyl)- 2,3-dioxo-6-nitro-1,2,3,4-tetrahydrobenzo[f] quinoxaline-7-sulfonamide

NMDA
N-methyl-D-aspartate

I-V

current-voltage

ON

olfactory nerve

RI

rectification index

SYM2206

1,2-dihydro-1-methyl-2-propylcarbamoyl-6,7-methylenedioxyphthalazine

TEA

tetraethylammonium chloride

TTX

tetrodotoxin

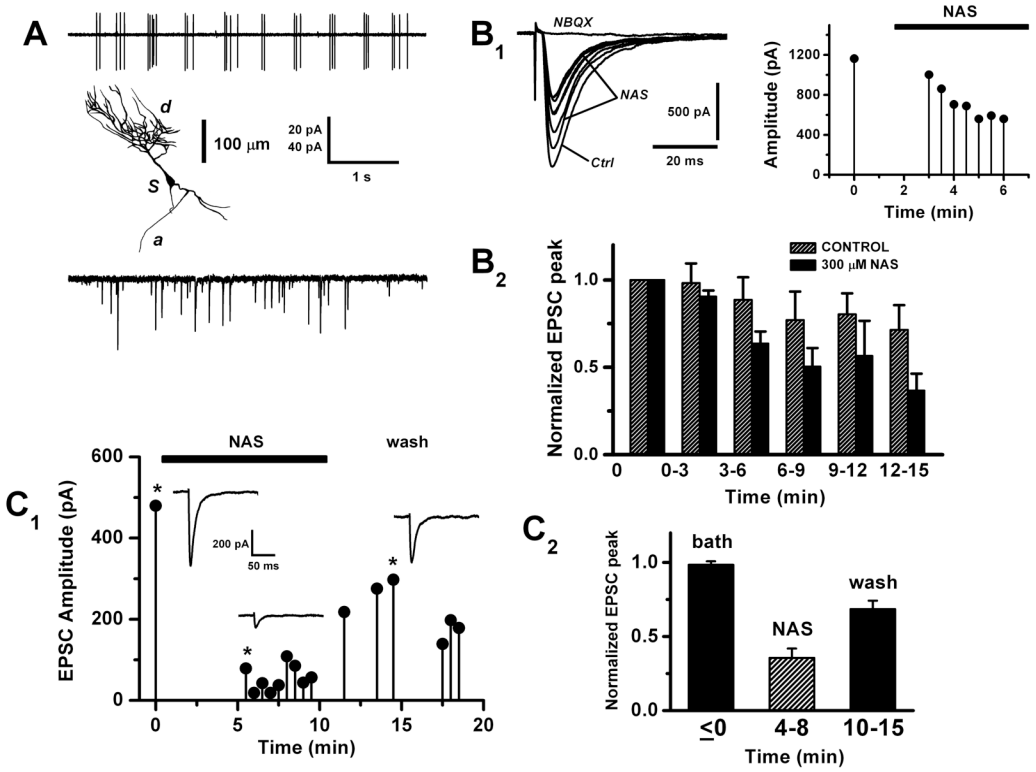

Figure 1. Olfactory nerve stimulation evokes an NAS-sensitive conductance in external tufted cells

A. Properties of external tufted (ET) cells in olfactory bulb slices. Upper panel: cell-attached voltage-clamp recording of capacitance currents from an ET cell soma, showing the characteristic spontaneous burst discharge. Middle panel: morphology of an ET cell recovered by biocytin staining; d, dendritic tuft; s, soma; a, axon. Lower panel: spontaneous excitatory postsynaptic currents (EPSCs) recorded in whole cell mode (− 60 mV). Slices were perfused with standard artificial cerebrospinal fluid and whole-cell recordings made with K methylsulfate based internal solution. Vertical scale bar 20 pA (upper panel), 40 pA (lower panel).

B. Polyamine block of the olfactory nerve shock-evoked EPSC in ET cells. B_1, left panel: a series of shock-evoked whole-cell currents (−60 mV), the first recorded initially in control bath solution (*Ctrl*), 7 responses subsequently recorded after switching to 300 μM 1-naphthyl acetyl-spermine (*NAS*); the last trace shows NBQX (1 μM) abolished the response. A stimulus artefact indicates the timing of olfactory nerve shock. B_1, right panel: plot of peak amplitude vs. time of the responses during wash in of NAS. The perfusion valve was switched at time = 0. B_2, summary plot showing the change in the average EPSC amplitude over time, following switch to NAS perfusion. Hatched bars: normal run down of the EPSC in control cells recorded without NAS perfusion (n = 7 cells). Filled bars: cells exposed to NAS (n = 12 cells). On the abscissa, time = 0 corresponds to about 5 min after patch rupture, to allow the recording and series resistance to stabilize. For each cell, amplitude of the EPSC was normalized to the response at time = 0. Bath contained 100 μM APV, 150 μM BMI, internal solution 10 mM QX314.

C. Recovery from polyamine block of the olfactory nerve shock-evoked EPSC. C_1: plot of peak amplitude vs. time of the EPSC after switch to NAS perfusion (black bar), then after NAS was washed out of the bath. The inset traces (control, NAS and wash) correspond to the plot data points marked with a star (*). C_2: summary plot showing the recovery of the EPSC after washing out NAS, normalized to time = 0 (n = 5 cells).

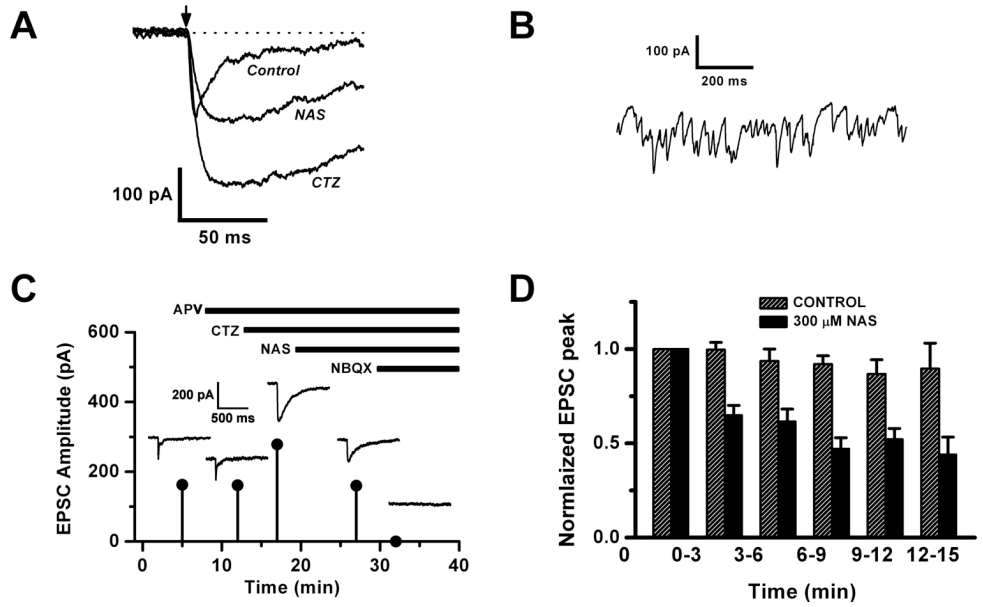

Figure 2. Glutamate uncaging evokes an NAS-sensitive conductance in external tufted cells

A. Rising phase and peak of the EPSC evoked by uncaging glutamate on the dendritic tuft of an ET cell. In the first trace labeled *Control*, the bath contained 100 μM APV to isolate an AMPA/kainate current. Second trace shows that addition of 100 μM cyclothiazide (*CTZ*) amplified the AMPA receptor component of the EPSC and prolonged both the time to peak and the decay. In the third trace, addition of 300 μM NAS attenuated the response 50%, leaving the kinetics unaltered. Bath contained 150 μM BMI, 150 μM Cd^{2+}, 1 μM TTX and 1 mM MNI-caged glutamate, uncaged with a nitrogen laser (300 μJ, 4 ns). Arrow shows timing of laser pulse.

B. Spontaneous EPSCs recorded from an ET cell in 100 μM CTZ. The bath also contained 1 μM TTX, 50 μM BMI, 15 μM dCK and 150 μM Cd^{2+}.

C. Plot of peak amplitude vs. time of the uncaging EPSC after successive administration of drugs: 100 μM APV, 100 μM CTZ, 300 μM NAS and 1 μM NBQX (same cell as shown in 2A). Insets show the actual traces recorded.

D. Summary plot showing the change in the average uncaging EPSC amplitude over time, following switch to NAS perfusion. Hatched bars: normal run down of the uncaging EPSC in control cells recorded without NAS perfusion (n = 18 cells). Filled bars: cells exposed to 300 μM NAS (n = 13 cells, 9 recorded by whole-cell, 4 by perforated patch). Time = 0 corresponds to about 5 min after patch rupture, and amplitudes were normalized to this time point. Bath solution contained 15 μM dCK or 100 μM APV, 150 μM BMI, internal solution 10 mM QX314. Uncaging data obtained from using flash lamp and nitrogen laser are pooled.

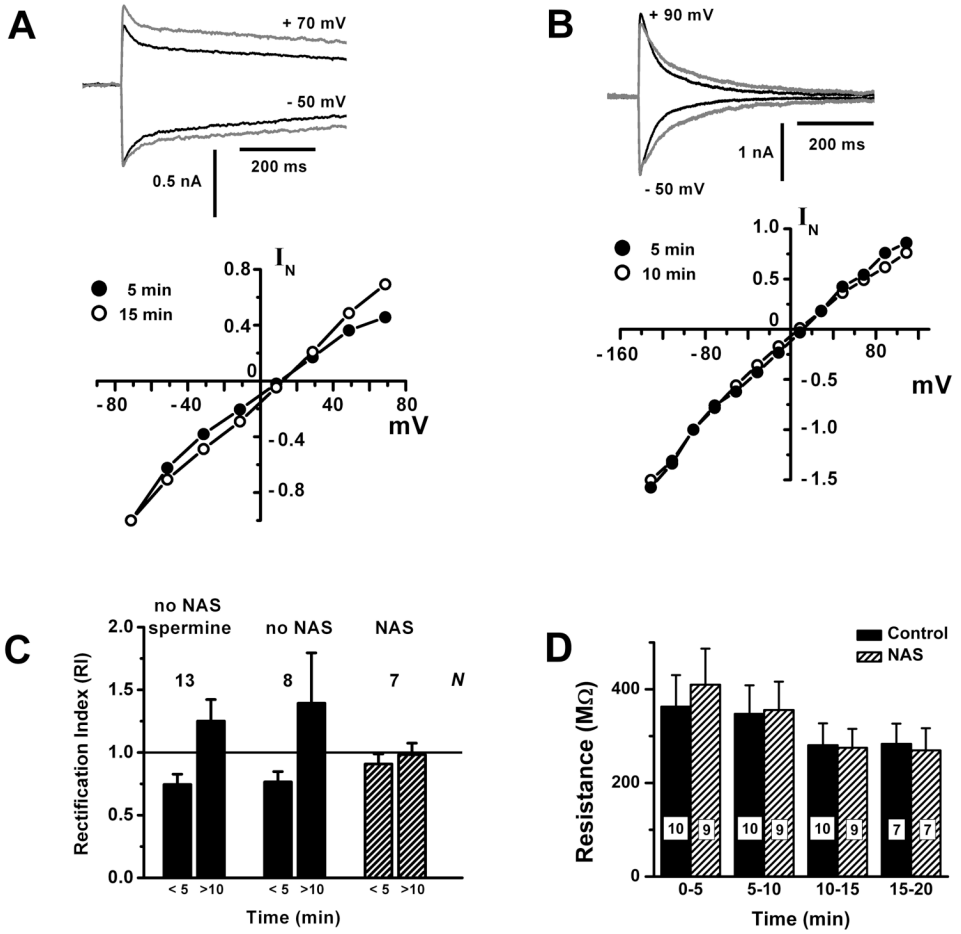

Figure 3. Glutamate uncaging evokes an inwardly rectifying conductance in external tufted cells

A. Weak inward rectification is lost over time. Upper panel: plots of inward and outward uncaging currents (− 50 mV and +70 mV) recorded at 5 min (black trace) and 15 min (gray trace) after patch rupture. Lower panel: I-V curves obtained at 5 min (filled circles) and 15 min (open circles), showing loss of inward rectification. EPSC amplitudes were normalized to the values at − 71 mV. Bath solution contained 500 μM MNI-caged glutamate, 15 μM dCK, 50 μM BMI, 1 μM TTX, 20 mM TEA, 300 μM Cd^{2+}.

B. Weak inward rectification is absent in NAS. Upper panel: plots of inward and outward uncaging currents (− 50 mV and +90 mV) recorded at 5 min (black trace) and 10 min (gray trace) after patch rupture. Lower panel: I-V curves obtained at 5 min (filled circles) and 10 min (open circles), showing lack of inward rectification or wash out effects. EPSC amplitudes were normalized to the values at − 71 mV. Bath solution as in 3A, but with 300 μM NAS.

C. Summary of the changes in rectification index (RI) of I-V curves obtained at early (< 5 min) and late (> 10 min) times, in the absence (filled bars) or presence (hatched bars) of NAS. In the former group, also shown are results from a group in which 75 – 250 μM spermine included in the internal solution did not delay the loss of inward rectification. Number of cells (*N*) is indicated for each group.

D. Average cell input resistance (MΩ) at different times after establishing a whole-cell recordings from ET cells, either with (hatched bars) or without (solid bars) wash-in of 300 μM NAS. Control bath solution was the same as in 3A. For the wash-in trials (hatched), the NAS concentration in the bath was stable after > 5 min. Input resistance was obtained from applying −30 mV hyperpolarizing pulses from a holding potential of − 60 mV, without

compensating series resistance (8 – 10 MΩ pipette). Numerical labels on the bars indicate the number of cells in each measurement.

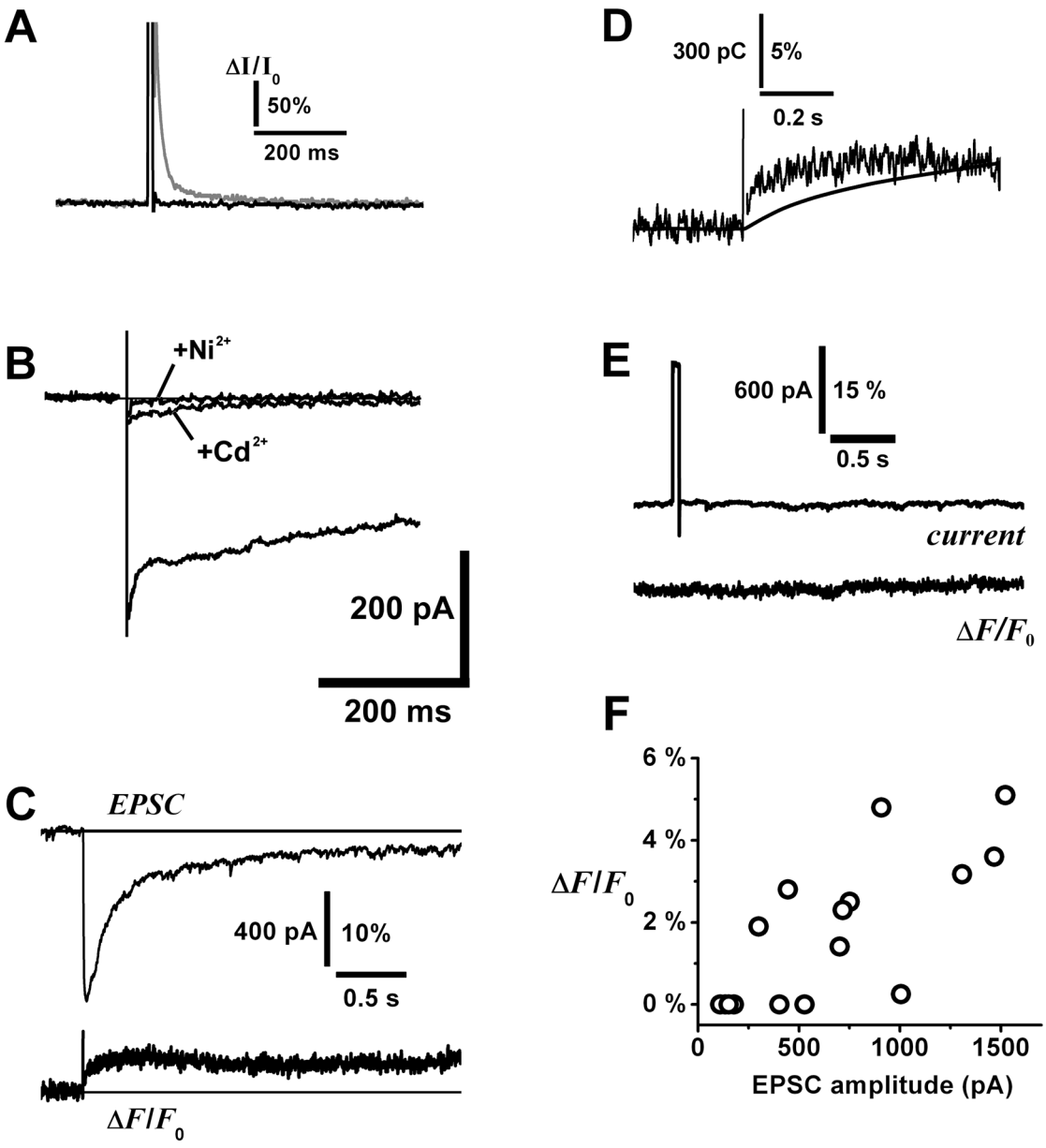

Figure 4. Fluorometric measurement of calcium transients evoked by glutamate uncaging in external tufted cells

A. Photodiode control responses to laser uncaging flash. At higher laser power (10 mW at focal plane), the flash induced a slow transient artifact (gray trace) in the detector. We adjusted laser power to a range (0.25 – 0.5 mW) that was sufficient to uncage glutamate and evoke large EPSCs without generating the slow artifact (black trace). $\Delta I/I_0$ = relative change in detector current over baseline current I_0.

B. Block of voltage-activated Ca^{2+} currents in an ET cell. The lower trace is the Ca^{2+} current in control condition (HEPES buffered bath solution with 1 μM TTX, 3 mM Cs^+, 3 mM 4-aminopyridine, 40 mM TEA; Cs-methanesulfonate internal solution), the middle trace after addition of 150 μM Cd^{2+}, and the upper flat trace with 150 μM Cd^{2+} and 250 μM Ni^{2+}. Currents were activated under voltage clamp by stepping from − 60 mV to 0 mV. A whole-cell

capacitance transient was subtracted from the records, and an imperfectly cancelled transient (< 10 ms) has been blanked from the traces. Similar data were obtained from *n* = 2 ET cells.
C. Upper trace: AMPA/kainate EPSC evoked by uncaging glutamate on the soma and proximal dendrite of an ET cell. Lower trace: relative fluorescence change $\Delta F/F_0$ in fluo-4 detected by photodiode, fluorescence was spatially summed over the soma and proximal dendrite, the area illuminated by the arc lamp.
D. Overlay of the rising phases of $\Delta F/F_0$ and integrated charge of the EPSC in 4C.
E. Absence of detectable fluo-4 fluorescence change after applying a 50 ms depolarizing voltage pulse (− 60 mV to 0 m V) to an ET cell to test for activation of voltage-gated Ca^{2+} channels in 200 μM Cd^{2+}. This same cell responded to glutamate uncaging with a large EPSC and a sustained fluorescence transient, similar to 4C.
F. Correlation plot of peak amplitude of fluo-4 fluorescence signal against peak amplitude of AMPA/kainate EPSC (data from *n* = 12 cells).

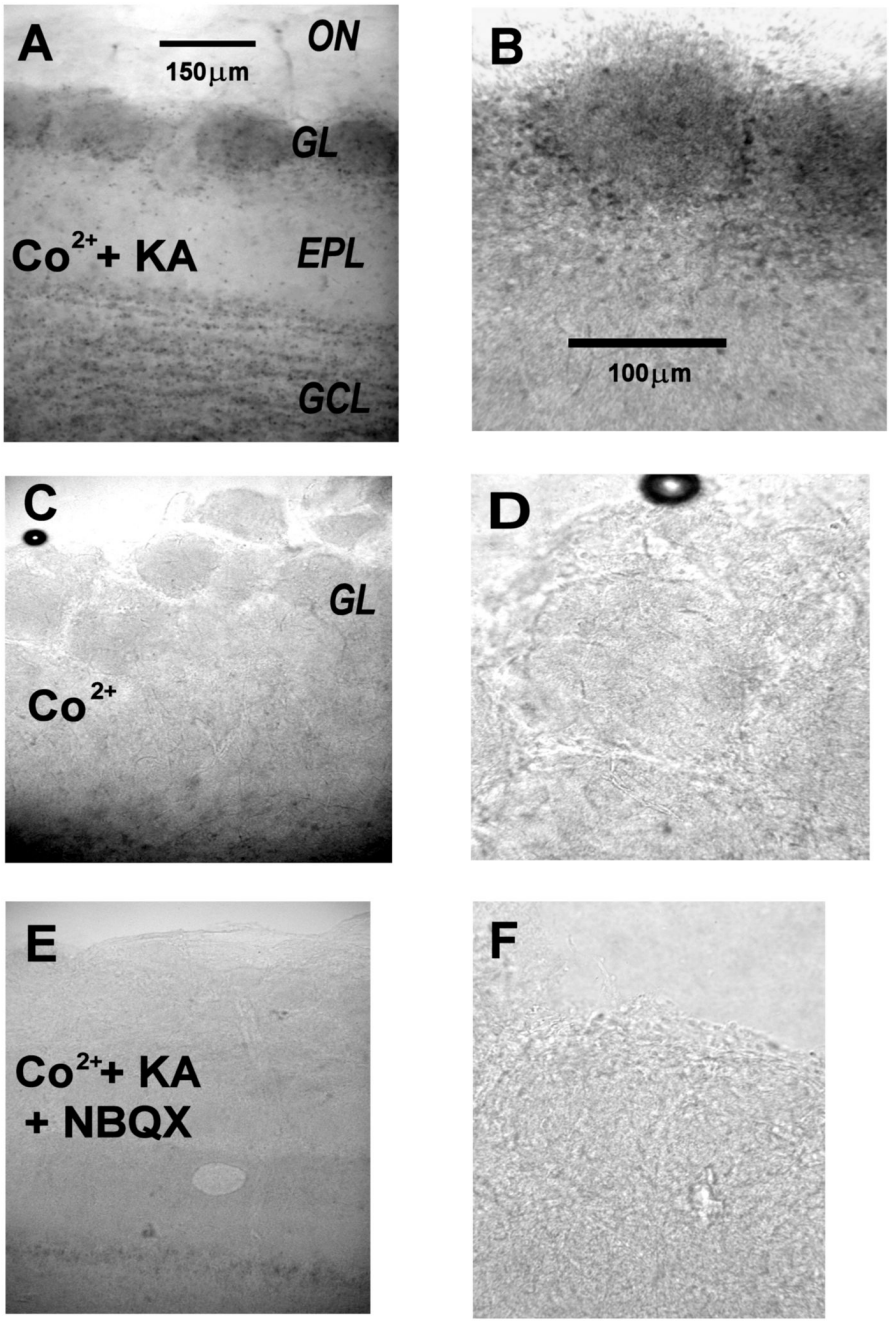

Figure 5. AMPA/kainate receptor-dependent cobalt uptake in the glomerular layer of the olfactory bulb

A, B: Horizontal olfactory bulb slices were exposed in vitro to 250 μM kainate (KA) in the presence of 5 mM $CoCl_2$ (CO). After fixing, the slices were stained for cobalt by treatment with ammonium sulfide, which precipitates cobalt sulfide (dark areas). A: low magnification of a treated slice, showing strong staining of glomeruli (*GL*, dark ovoid regions on the left). The olfactory nerve layer (*ON*) was unstained, the external plexiform layer (*EPL*) weakly and the granule cell layer (*GCL*) more strongly stained. Scale bar: 150 μm. B: At higher magnification, staining of individual juxtaglomerular cell somata can be discerned. Scale bar: 100 μm.

C, D: Low (C) and high (D) magnification views of a control slice treated with cobalt, without kainate stimulation. No staining is apparent. Scales as in 5A, 5B.
E, F: Low (E) and high (F) magnification views of a control slice treated with cobalt, stimulated with kainate and with 100 μM NBQX to completely block AMPA/kainate receptors. No staining is apparent. Scales as in 5A, 5B.

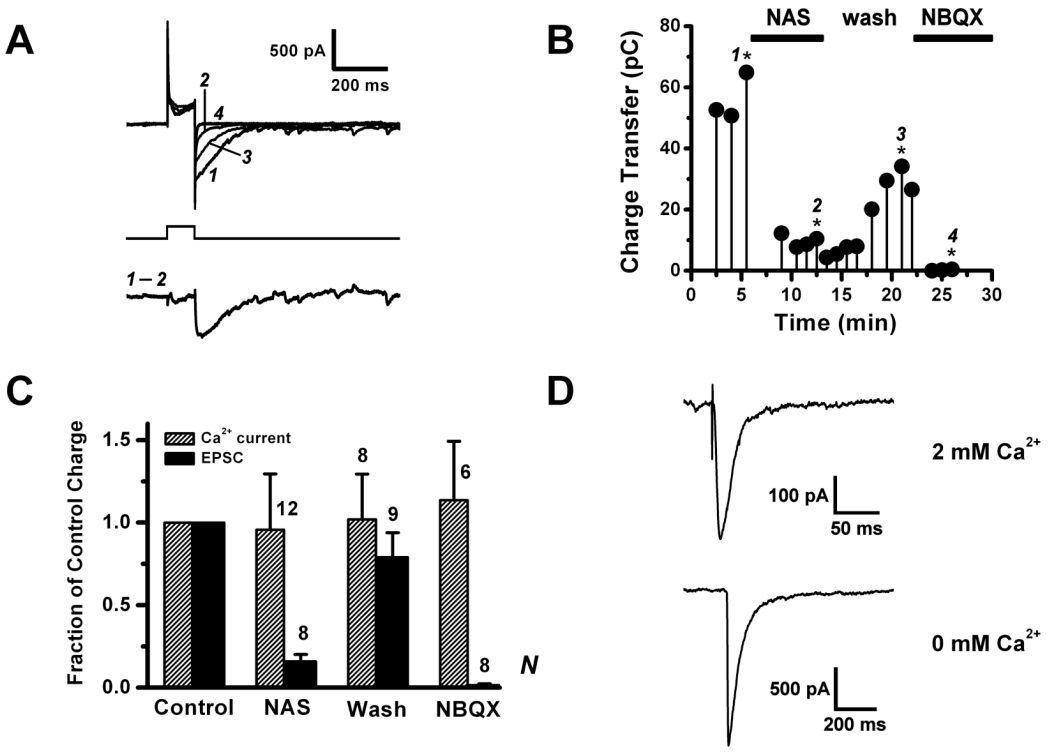

Figure 6. A polyamine sensitive AMPA autoreceptor in external tufted cells

A. Tail current evoked by voltage pulse depolarization (−60 to 0 mV, 100 ms) of an ET cell to trigger dendritic release of glutamate. Upper traces: a sequence of tail currents; control (*1*), after perfusion with 300 μM NAS (*2*), after wash out of NAS (*3*), and after addition of 10 μM NBQX (*4*). Lower trace: The NAS-sensitive component of the tail current, isolated by digital subtraction of traces *1* and *2* in A. The bath contained 15 μM dCK, 150 μM bicuculline, 2 mM TEA, 1 μM TTX and 100 μM CTZ. The internal solution contained CsMeSO4 and 30 mM L-glutamate.

B. Plot of charge transfer vs. time of the tail current, after subtraction of the capacitance charge transfer estimated in 10 μM NBQX, for the cell in A. The labeled data points (with stars) correspond to traces 1 – 4 in 6A.

C. Summary plot comparing charge transfers of the tail current and the calcium current (calculated during the 0 mV pulse) in the control condition, under NAS perfusion, after NAS wash out, and in NBQX. The Ca^{2+} current was unaffected by NAS, whereas the tail current was strongly suppressed.

D. Inward currents evoked by intracellular flash photolysis of caged calcium (DM-Nitrophen). Upper trace was recorded in external solution containing 2 mM Ca^{2+}, lower trace in 0 mM external Ca^{2+}. Bath solution contained 500 μM Cd^{2+}, 26 mM NaHEPES, and CTZ was omitted.